MOLECULAR AND CELLULAR BIOLOGY, Jan. 2011, p. 138–150 Vol. 31, No. 1
0270-7306/11/$12.00 doi:10.1128/MCB.00709-10

Global Profiling and Molecular Characterization of Alternative Splicing Events Misregulated in Lung Cancer▽†

Christine M. Misquitta-Ali,[1] Edith Cheng,[2] Dave O'Hanlon,[1] Ni Liu,[3] C. Jane McGlade,[4] Ming Sound Tsao,[3,5] and Benjamin J. Blencowe[1,6]*

Banting and Best Department of Medical Research, University of Toronto, Donnelly Centre, 160 College Street, Toronto, Ontario, Canada M5S 3E1[1]; Department of Biochemistry, University of Toronto, 1 King's College Circle, Toronto, Ontario, Canada M5S 1A8[2]; University Health Network, Ontario Cancer Institute and Princess Margaret Hospital Site, 610 University Avenue, Toronto, Ontario, Canada M5G 2M9[3]; Arthur and Sonia Labatt Brain Tumor Research Centre, Hospital for Sick Children, and Department of Medical Biophysics, University of Toronto, Toronto Medical Discovery Tower, MaRS Centre, 101 College Street, Toronto, Ontario, Canada M5G 1L7[4]; Department of Laboratory Medicine and Pathobiology, University of Toronto, 1 King's College Circle, Toronto, Ontario, Canada M5S 1A8[5]; and Department of Molecular Genetics, University of Toronto, 1 King's College Circle, Toronto, Ontario, Canada M5S 1A8[6]

Received 20 June 2010/Returned for modification 19 July 2010/Accepted 25 October 2010

Alternative splicing (AS) is a widespread mechanism underlying the generation of proteomic and regulatory complexity. However, which of the myriad of human AS events play important roles in disease is largely unknown. To identify frequently occurring AS events in lung cancer, we used AS microarray profiling and reverse transcription-PCR (RT-PCR) assays to survey patient-matched normal and adenocarcinoma tumor tissues from the lungs of 29 individuals diagnosed with non-small cell lung cancer (NSCLC). Of 5,183 profiled alternative exons, four displayed tumor-associated changes in the majority of the patients. These events affected transcripts from the *VEGFA*, *MACF1*, *APP*, and *NUMB* genes. Similar AS changes were detected in *NUMB* and *APP* transcripts in primary breast and colon tumors. Tumor-associated increases in *NUMB* exon 9 inclusion correlated with reduced levels of NUMB protein expression and activation of the Notch signaling pathway, an event that has been linked to tumorigenesis. Moreover, short hairpin RNA (shRNA) knockdown of NUMB followed by isoform-specific rescue revealed that expression of the exon 9-skipped (nontumor) isoform represses Notch target gene activation whereas expression of the exon 9-included (tumor) isoform lacks this activity and is capable of promoting cell proliferation. The results thus reveal widespread AS changes in NSCLC that impact cell signaling in a manner that likely contributes to tumorigenesis.

Alternative splicing (AS), the process by which splice sites are differentially utilized to produce different mRNA isoforms, is a major step in the generation of proteomic and functional diversity in metazoans. At least 95% of human multiexon genes generate alternatively spliced transcripts, and the majority of these vary in level between different cell and tissue types (35, 53). Previous studies have provided evidence that AS and the RNA binding proteins and other factors which control this process are often deregulated in cancers and other human diseases (7, 14, 15, 17, 49, 51).

In order to better understand the mechanisms underlying tumorigenesis, a critical goal is to identify consistent molecular changes underlying the initiation and progression of cancers. Such molecular changes represent promising candidates for diagnostic and therapeutic applications (15, 39, 56). Since AS often regulates subsets of genes that are not coregulated at the transcriptional level (31, 36), profiling of this layer of gene regulation has tremendous potential to identify molecular markers of cancer that are missed by other methods (3). For example, in the case of prostate cancer, it has been shown that AS signatures derived from microarray-based profiling are more reliable for diagnostic purposes than are signatures derived from mRNA expression profiling (61). Other studies have recently employed high-throughput reverse transcription-PCR (RT-PCR)-based screening of splicing changes in breast and ovarian tumor samples and have also revealed tumor-associated splicing signatures of potential diagnostic and prognostic value (27, 50).

Lung cancer is the most common cause of mortality among all cancers, accounting for an estimated 1.3 million deaths annually (42). Non-small cell lung cancer (NSCLC) is the most prevalent and heterogeneous subtype of lung cancer, comprising adenocarcinoma, squamous cell carcinoma, and large cell carcinoma. Adenocarcinoma is frequently associated with lung cancer in smokers, but it is also the most common type of lung cancer type in nonsmokers (46).

In this study, we performed a large-scale screen for AS changes between matched normal and adenocarcinoma tumor tissue from NSCLC patients. Our results reveal that of several thousand cassette-type alternative exons profiled using a custom microarray, four display pronounced and consistent tumor-associated changes in the majority of patients analyzed. The most prevalent tumor-associated changes occurred in transcripts from genes with functions in angiogenesis, actin cytoskeleton remodeling, and Wnt/Notch signaling, namely, vascular endothelial growth factor A (VEGFA), microtubule-

* Corresponding author. Mailing address: 160 College Street, Room 1016, University of Toronto, Toronto, Ontario M5S 3E1, Canada. Phone: (416) 978-3016. Fax: (416) 946-5545. E-mail: b.blencowe@utoronto.ca.

† Supplemental material for this article may be found at http://mcb.asm.org/.

▽ Published ahead of print on 1 November 2010.

actin cross-linking factor 1 (MACF1), amyloid beta (A4) precursor protein (APP), and the Numb (*Drosophila melanogaster*) homolog (NUMB). Increased inclusion of exon 9 in transcripts from the NUMB gene was the most widespread tumor-associated AS event and was detected at the protein level. It was also correlated with decreased overall expression of the NUMB protein, activation of Notch target genes, and increased cell proliferation (22, 57). These findings provide mechanistic insight into how AS changes may contribute to tumorigenesis in NSCLC and other cancers and further reveal markers of potential clinical value.

MATERIALS AND METHODS

Patient samples, cell lines, and cell culture. Matched pairs of primary tumor and adjacent normal tissue samples were obtained from the lungs of 29 adenocarcinoma patients (see Table S1 in the supplemental material for details). Matched pairs of normal and tumor tissue samples from breast and colon were obtained from the Ontario Institute of Cancer Research (OICR) Tumor Bank (see Table S2). All tissue samples were flash frozen within 30 min after surgical removal and stored at −80°C until further use. A549 cells were grown in RPMI (Sigma) with 10% fetal bovine serum (FBS) and antibiotics (Pen-Strep) and incubated at 37°C with 5% CO_2.

RNA samples and isolation. Total RNA was extracted from lung tissue samples using guanidium thiocyanate-phenol-chloroform extraction (13). Poly(A)$^+$ RNA was isolated using the NucleoTrap mRNA extraction kit (Clontech), as per the manufacturer's instructions. Frozen breast and colon tissue samples were homogenized with a Tissue Tearor homogenizer in the presence of TRI Reagent (Sigma) prior to RNA extraction. RNA concentrations were determined using a ThermoScientific NanoDrop spectrometer. Samples of normal human tissue poly(A)$^+$ RNA (each pooled from multiple individuals) analyzed in Fig. 2 were purchased from Clontech.

Microarray hybridization and data analysis. Poly(A)$^+$ RNA isolated from tissue samples from 10 lung cancer patients (see Table S1 in the supplemental material) was amplified essentially as previously described (10), and cDNA samples from each tissue were synthesized with cyanine 3 and cyanine 5 fluorescent dyes in separate reactions. Labeled cDNAs were hybridized to a custom-designed human oligonucleotide microarray (manufactured by Agilent Technologies Inc.) containing probe sets for monitoring 5,183 unique cassette-type AS events, as previously described (9). Microarrays were scanned using an Agilent 2100 scanner, and images were processed and normalized as previously described (36). Preprocessed probe intensity values were analyzed using the GenASAP algorithm to generate confidence-ranked predictions for percent exon inclusion levels for each cassette alternative exon (36, 44).

RT-PCR assays. Primer pairs matched for melting temperature (T_m) and AT/GC content and complementary to exons flanking each cassette alternative exon were used to simultaneously amplify exon-included and -skipped isoforms. All RT-PCRs were performed in the presence of [α^{32}P]dCTP using the One-Step kit (Qiagen) as previously described (9). Reaction products were resolved using 5% denaturing polyacrylamide-urea gels. Isoform expression levels were quantified using a Typhoon Trio PhosphorImager and ImageQuant software (GE Healthcare). Percent exon inclusion levels were calculated as the percentage of the isoform including an alternative exon divided by the total abundance of the two isoforms including and excluding the alternative exon. All primer sequences used in this study are available upon request.

Protein extraction and Immunoblotting. Normal and tumor tissue samples were homogenized in RIPA buffer (50 mM Tris-Cl [pH 7.4], 150 mM NaCl, 0.25% deoxycholic acid, 1% NP-40, 1 mM EDTA containing Complete mini, EDTA-free protease inhibitor cocktail [Roche] plus 1.5 mM phenylmethylsulfonyl fluoride [PMSF] plus 1 mM dithiothreitol [DTT]) using a Tissue Tearor homogenizer. Extracts were sonicated three times for 7 s with 30 s on ice between bursts. Lysates were collected following removal of insoluble material from the tissue extracts by high-speed centrifugation for 20 min at 4°C. Samples were boiled in Laemmli buffer, separated on 8% SDS polyacrylamide gels, and transferred to a polyvinylidene difluoride (PVDF) membrane using semidry transfer. Immunoblotting was performed as previously described (5). Analysis of NUMB isoforms was performed using rabbit anti-NbA (specific for all NUMB but not NUMB-like proteins) and rabbit anti-Nb#11 (specific for exon 9-included [proline-rich-region [PRR]-long {PRR^L}] isoforms) (18). Monoclonal anti-α-tubulin antibody was purchased from Sigma Inc.

Cloning, transfection, and infection. Coding regions of NUMB isoforms including or excluding exon 9 were amplified by PCR from full-length cDNA plasmids (18) and subcloned into the pcDNA 3.1 vector using the KpnI and XhoI restriction sites. A Kozak sequence and Myc tag were included upstream of the NUMB coding sequence in each plasmid to create myc-NUMB-exon9-plus and myc-NUMB-exon9-minus, respectively. Both constructs included alternative exon 3. Plasmids containing exon 9-included NUMB (myc-NUMB-exon9-plus) and exon 9-excluded NUMB (myc-NUMB-exon9-minus) were transfected into A549 cells (plated at 100,000 cells/ml) using 2 μl TurboFect transfection reagent (MBI Fermentas) per μg DNA, according to the manufacturer's protocol. Empty pcDNA plasmid was used as a control in all transfections. RNA and protein were harvested as described above, 48 h posttransfection.

Short hairpin RNA (shRNA) knockdown of NUMB was achieved by infecting A549 cells with lentivirus particles (Dharmacon) containing shRNA targeting the sequence: GTTGTATGAGTTGTAAGTA, located in the 3′ untranscribed region (3′-UTR) of NUMB. Cells containing virus were selected with puromycin at a concentration of 1 μg/ml growth medium and using a multiplicity of infection (MOI) determined to result in knockdown of all NUMB isoforms. In parallel, A549 cells were infected with a control virus expressing shRNA specific for green fluorescent protein (GFP) at a comparable MOI.

Isoform-specific rescue plasmids were constructed by subcloning the coding region of NUMB (as described above) into the pWZL-hygro plasmid (8) using the EcoRI and SalI restriction enzyme sites to create the myc-NUMB-exon9-minus-hygro and myc-NUMB-exon9-plus-hygro plasmids. Phoenix cells (Orbigene) were transfected with the myc-NUMB-exon9-minus-hygro, myc-NUMB-exon9-plus-hygro, and control–WZL-hygro plasmids to produce virus particles as previously described (8). The stable NUMB knockdown line (shNUMB) and stable GFP control knockdown line (shGFP) were then infected at various MOIs with a control virus and viruses for expressing the myc-NUMB-exon9-minus-hygro and myc-NUMB-exon9-plus-hygro viruses. All lines were selected with hygromycin at 750 mg/ml and puromycin at 1 μg/ml medium. RNA and protein lysates were harvested from infected cells as described above in order to determine which MOI was effective in restoring expression of each of the splice isoforms of NUMB.

Cell proliferation assays. The cell lines described above stably expressing shRNA to knock down all NUMB isoforms, with and without cDNAs for expression of NUMB isoforms, were seeded in 96-well plates at a density of 20,000 cells/ml and harvested for cell proliferation assays at days 1, 3, and 6 postseeding. Wells containing medium but lacking cells were monitored in parallel as a background control. On each day of cell growth determination, WST-1 (Roche Diagnostics) was added to the wells according to the manufacturer's instructions, and plates were incubated at 37°C for 30 min (determined to be optimal in preliminary assays with A549 cells). Plates were read at room temperature in an enzyme-linked immunosorbent assay (ELISA) plate reader at 450 nM (for growth determination) or 650 nM (for reference).

RESULTS

Microarray detection of misregulated AS events in lung adenocarcinoma. In order to detect AS-level differences between patient-matched pairs of lung adenocarcinoma tumor tissue and adjacent normal lung tissue, we performed quantitative AS profiling (36, 44) of 5,183 cassette-type alternative exons using poly(A)$^+$ RNA isolated from samples from 10 individuals (Fig. 1A). Using this system, confidence-ranked estimates for percent exon inclusion levels (i.e., the percentage of transcripts with exon inclusion; denoted below as "%In") were generated. Gene information and estimates for %In values for the profiled exons are provided elsewhere (see http://www.utoronto.ca/intron/LungCancer/Christine_Manuscript_suppl_table3.xls).

A change in exon inclusion level of ~10 percentage points can have important consequences for disease pathology (21) but is close to the detection sensitivity limit of our microarray system (34, 36). Accordingly, to maximize the detection of tumor-associated AS changes, we used our microarray data to predict exons with %In changes of at least 10 percentage points between normal and tumor samples in 5 or more of the 10 profiled patients.

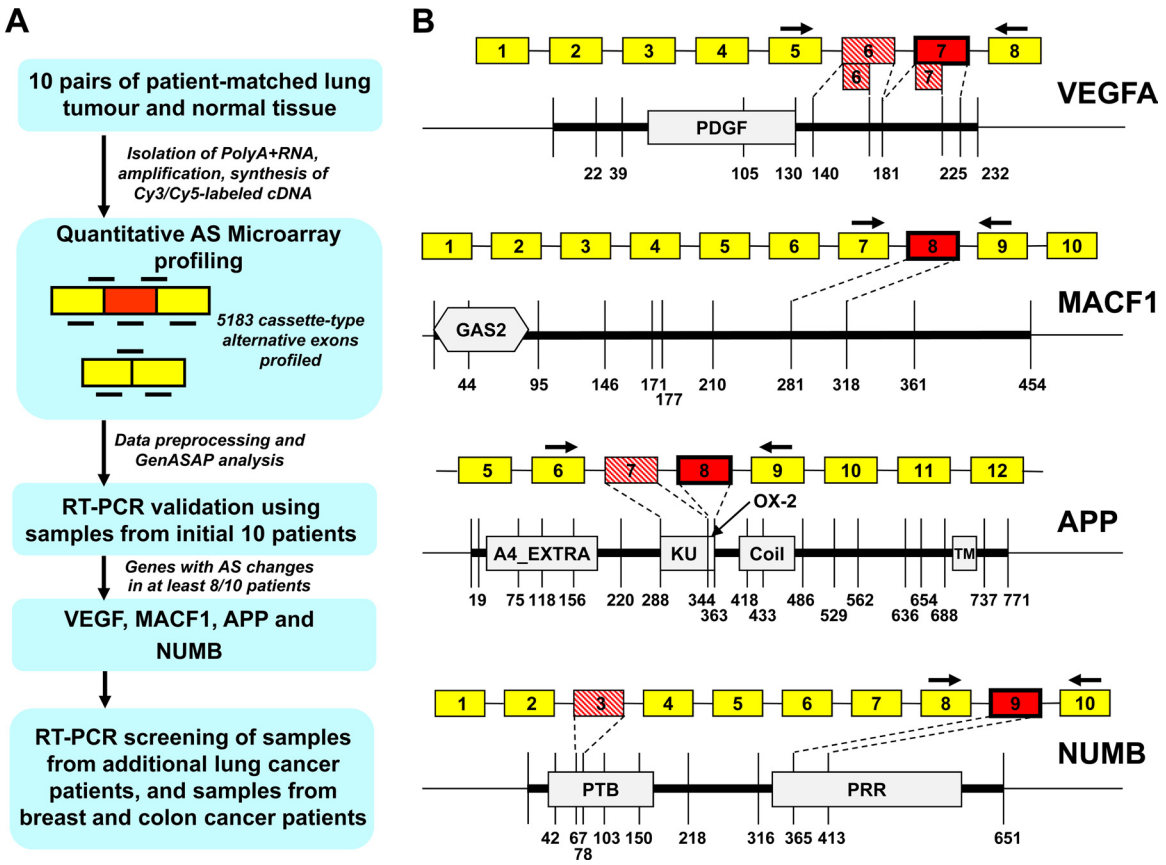

FIG. 1. Detection of alternative splicing events misregulated in non-small cell lung cancer (NSCLC). (A) Overview of strategy. Poly(A)$^+$ RNA isolated from patient-matched pairs of normal lung tissue and adenocarcinoma tumor tissues was analyzed by quantitative AS microarray profiling, and frequently detected changes in cassette-type AS events were validated by RT-PCR assays. Following initial validation of consistent AS changes, further validation and analysis were performed with additional NSCLC adenocarcinoma patients and samples from other cancer types. (B) Genes showing consistent AS changes in the lung adenocarcinoma samples. Alternative exons with tumor-dependent AS changes are shown in solid red; additional AS events are indicated by red shading. Genomic coordinates of the constitutive and alternative exon for each event can be found in Fig. S1 in the supplemental material. Domain organization of each protein with amino acid coordinates is indicated to scale. Protein coding regions are indicated with bold lines, and untranslated regions are indicated with thin lines. VEGFA, vascular endothelial growth factor A; MACF1, microtubule-actin cross-linking factor 1; APP, amyloid beta (A4) precursor protein; NUMB, Numb (*Drosophila*) homolog; PDGF, platelet-derived and vascular endothelial growth factor family domain; GAS2, growth arrest-specific protein 2 domain; A4_EXTRA, amyloidogenic glycoprotein extracellular domain signature; KU, BPTI/Kunitz family of serine protease inhibitors domain; OX-2, MRC OX-2 antigen domain; Coil, coiled coil region; TM, transmembrane domain; PTB, phosphotyrosine-binding domain; PRR, proline-rich region.

Based on prior experience, we expected a relatively high (~50%) false-positive rate when predicting %In level changes of 10 percentage points or greater, since only changes of 15 percentage points or higher typically resulted in RT-PCR validation rates of at least 80% by our system (34, 36). Moreover, we also expected a higher-than-normal false-positive detection rate because it was necessary to introduce an RNA amplification step in our protocol (due to limited amounts of biopsy material), whereas in previous studies, unamplified poly(A)$^+$ RNA was used as a starting point. Consistent with these expectations, of a total of nine AS events predicted by the microarray data to meet the above selection criteria, four were validated as having tumor-associated AS changes in more than half of the patients. In fact, the RT-PCR assays demonstrated that these four AS events changed for 8 or more of the 10 patients (see below). The remaining five AS events did not display appreciable changes in AS levels (data not shown). Most of the tumor-associated inclusion level changes observed for the four validated AS events were determined by the RT-PCR assays to be in the range of 15 to 30 percentage points (Fig. 2 and 3).

To assess the false-negative detection rate of our microarray analysis, we randomly selected 20 AS events in genes that met our minimal cutoffs for expression and confidence-ranked estimates for percent exon inclusion levels. RT-PCR analysis of these AS events in the 10 patient-matched normal and tumor samples revealed that one AS event (in the *LBD2* gene) displayed a tumor-associated change in 5 of the 10 patients (data not shown). These results indicate that our profiling data and analysis afforded high detection sensitivity for tumor-associated AS events that occur in at least half of the profiled patients.

The four lung adenocarcinoma-associated AS events detected in our initial screen of 10 patients affect exon 7 in transcripts encoding vascular endothelial growth factor A (VEGFA) (also known as VPF); exon 8 in microtubule-actin

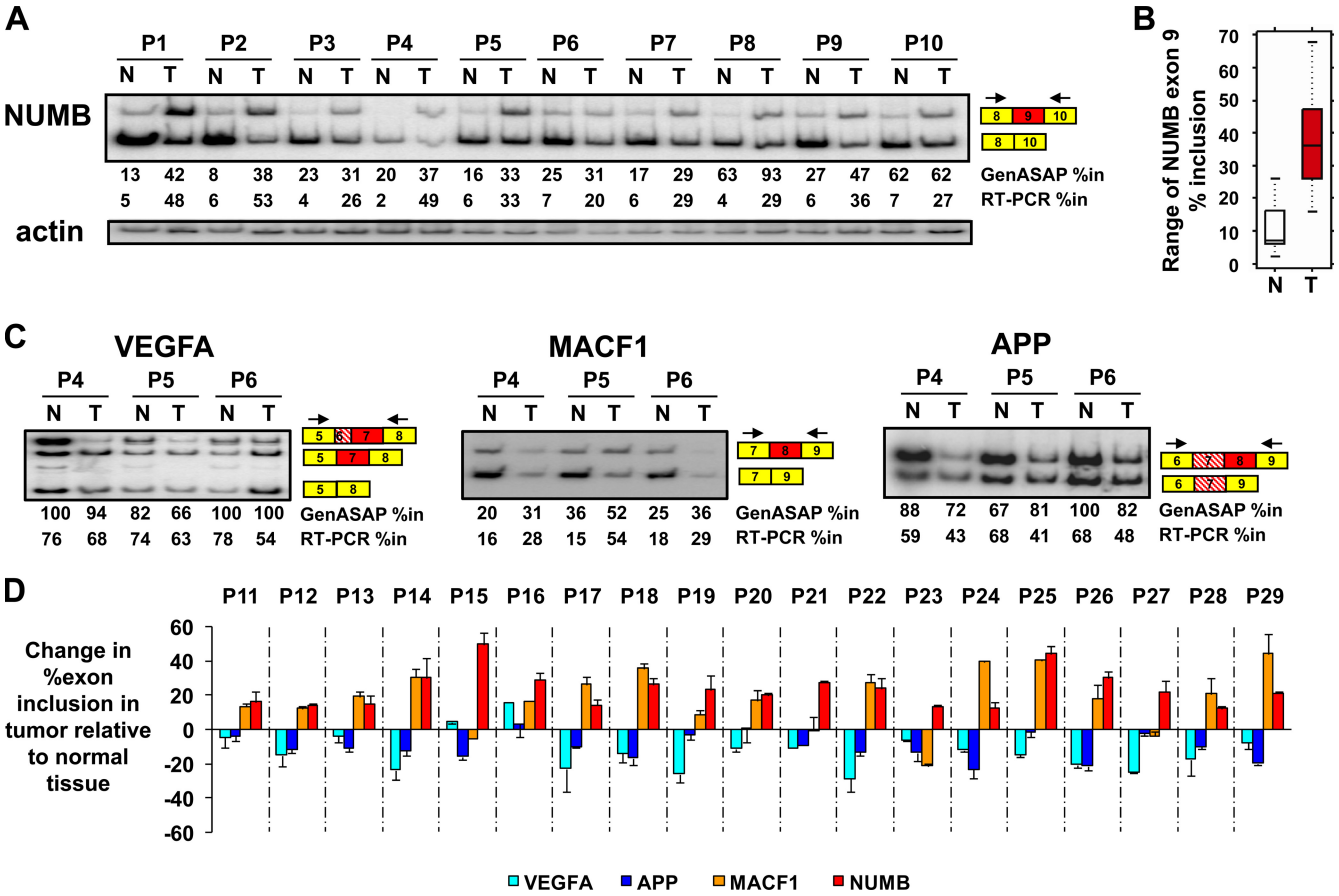

FIG. 2. Validation of microarray-detected AS changes in NSCLC patient samples. (A) RT-PCR validation of AS changes in exon 9 splicing of NUMB in patient-matched pairs of tumor (T) and normal (N) lung tissues from 10 individuals analyzed by microarray profiling. Values for % exon inclusion levels from microarray GenASAP predictions (GenASAP %In) and RT-PCR (RT-PCR %In) measurements are indicated. β-Actin expression is shown as a control for sample recovery and loading. (B) Box plot showing the distributions of %In levels of NUMB exon 9 in normal (N) and tumor (T) tissue samples from 29 patients (refer also to panel D). (C) Representative RT-PCR validation results for MACF1, VEGFA, and APP. (D) Bar plots showing average %In level changes between tumor and normal tissue detected by semiquantitative RT-PCR assays for 19 additional patient-matched pairs of normal lung and NSCLC adenocarcinoma tumor samples. Changes in %In values were determined as the mean values from three independent RT-PCR analyses, and standard deviations are indicated.

cross-linking factor 1 (MACF1) (also known as ACF7) transcripts, exon 8 in amyloid beta (A4) precursor protein (APP) transcripts, and exon 9 in Numb (*Drosophila*) homolog (NUMB) transcripts. Information on the function of these genes is provided in Discussion. Diagrams indicating the location of these alternative exons with respect to the domain organization of the corresponding translated products are shown in Fig. 1B, and exon coordinates are provided in Fig. S1 in the supplemental material. Interestingly, all four of the tumor-associated AS events are conserved between human and mouse transcripts, overlap coding sequences, and preserve the reading frame when included or skipped in mRNA. These properties are consistent with these exons normally having important physiological roles (see below and refer to Discussion) and the possibility that their misregulation might contribute to tumorigenesis. Results of RT-PCR validation experiments for the NUMB exon 9 AS event in all 10 pairs of patient samples are shown in Fig. 2A, and the range of the NUMB exon 9 %In levels in the patient-matched normal and tumor tissues is indicated in the box plot shown in Fig. 2B. Representative RT-PCR assays performed using a subset of the 10 patient samples are shown for the VEGFA, MACF1, and APP AS events in Fig. 2C.

Additional validation of AS changes in lung adenocarcinoma. In order to establish more conclusively whether the AS changes detected in transcripts from the above four genes are more widespread in NSCLC adenocarcinoma, we analyzed an additional 19 pairs of available matched patient tumor and normal lung tissue samples, using RT-PCR assays. Of these tumor-associated changes, the VEGFA AS event was detected in 12/19 (63%) individuals, the MACF1 event in 14/19 (74%) individuals, and the APP event in 13/19 (68%) individuals. Remarkably, the NUMB AS event was detected in all 19 pairs of samples. Quantification of these splicing changes from four independent RT-PCR assays is shown in Fig. 2D. These results provide evidence that the four AS events we detected in the initial 10 pairs of matched tumor and normal lung tissue samples occur in most NSCLC patients with adenocarcinoma and that the NUMB AS event is the most prevalent.

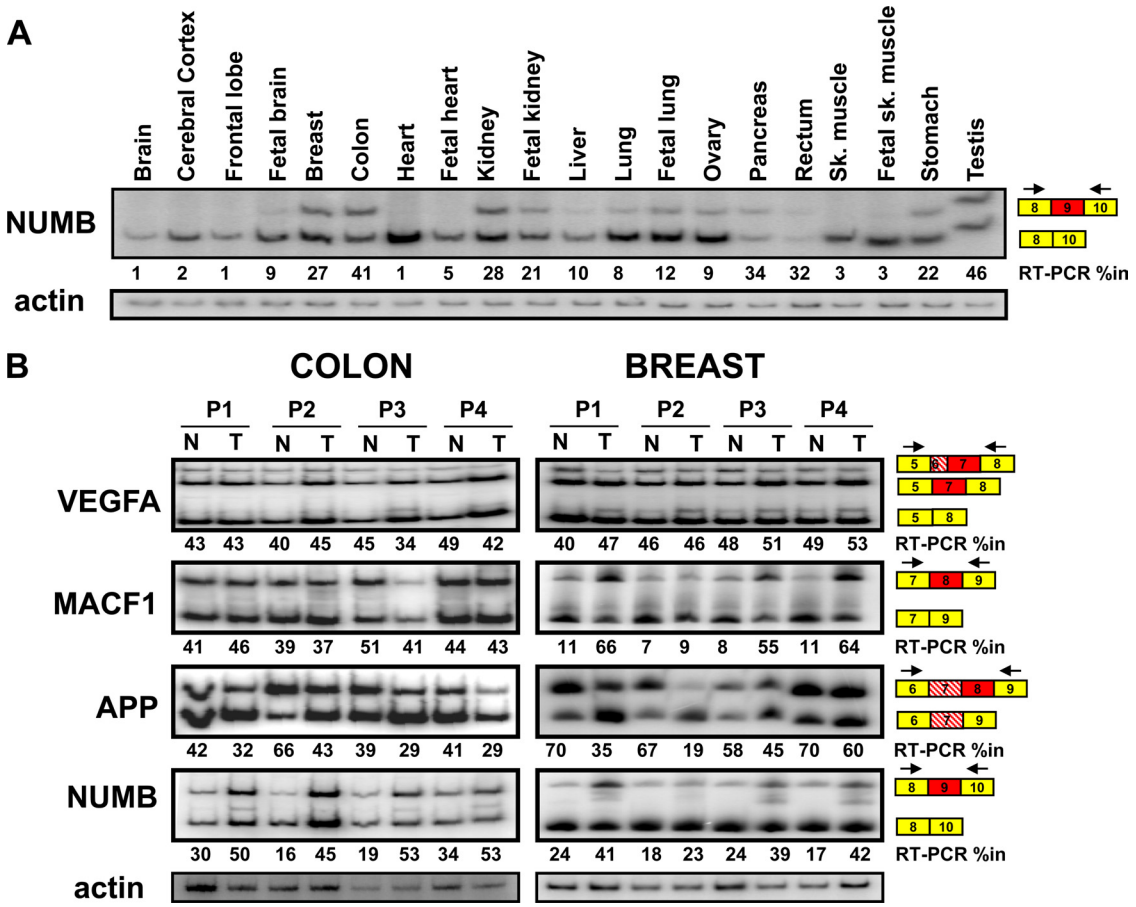

FIG. 3. NSCLC-associated AS events in other tissues. (A) Twenty diverse, normal human tissues were examined for NUMB exon 9 splicing by semiquantitative RT-PCR assays. The percent exon inclusion level (RT-PCR %In) in each tissue is shown. (B) Patient-matched pairs of normal (N) and tumor (T) samples from four colon and four breast cancer patients were analyzed by RT-PCR for changes in VEGFA, MACF1, APP, and NUMB AS. Percent exon inclusion levels quantified from the RT-PCR assays are indicated. β-Actin expression is shown as a control for sample recovery and loading.

Tissue specificity of tumor-associated AS events. In order to assess the specificities of the four AS events described above for lung adenocarcinoma tumor tissue, we examined whether they occur in mRNA samples from 20 physiologically diverse normal tissues (Fig. 3). Using RT-PCR assays, we found that one or both of NUMB exon 9-included or -skipped mRNA isoforms are expressed in all 20 tissues. However, in most normal tissues the ratio of the exon 9-included isoform to the exon 9-skipped isoform was lower than that observed in most tumor tissues (Fig. 3A). In a small subset of tissues, including breast, colon, kidney, pancreas, rectum, and testis, the levels of exon 9 inclusion were comparable to those observed in the majority of the lung adenocarcinoma tissues. Similarly, for the VEGFA, MACF1, and APP AS events, a subset of tissues displayed isoform expression ratios that were also comparable to those detected in the lung adenocarcinoma samples (see Fig. S2 in the supplemental material). However, it is possible that these tissues naturally require levels of isoforms that compare with those in lung adenocarcinoma, whereas tumors derived from these tissues might be associated with yet further increased levels of the tumor-associated isoforms detected in lung adenocarcinoma. To address this question and to determine whether the lung adenocarcinoma-associated AS changes also occur in other types of cancer, we next analyzed available matched normal and tumor tissue from breast and colon cancer patients.

Detection of AS changes in breast and colon cancer. Using RT-PCR assays, we analyzed the four lung adenocarcinoma-associated AS events in patient-matched normal and primary tumor tissue from four breast cancer and four colon cancer patients. Information on the types and origins of the tumor samples analyzed in these experiments is provided in Table S2 in the supplemental material.

In contrast to the lung adenocarcinoma samples, in which %In changes of 10 to 25 percentage points were detected for VEGFA exon 7 in more than half of the analyzed patients, only one of the four colon tumor samples displayed a comparable difference (~12 percentage points) in the splicing level. None of the breast tumor samples displayed %In changes in VEGFA exons 6 or 7 of >10 percentage points. MACF1 exon 8 did not show %In AS changes of more than 10 percentage points in any of the colon tumor samples but did display changes of at least this magnitude in three of the four breast tumor samples. In contrast, increased inclusion of NUMB exon 9 was detected

in all of the colon and all but one of the breast tumor samples relative to the corresponding patient-matched normal tissues, and APP exon 8 displayed %In changes of more than 10 percentage points in all of the colon and breast tumor samples (Fig. 3B).

Although our sample size is quite small, the results suggest that changes in the inclusion of exon 7 of VEGFA might be more specific to lung adenocarcinoma whereas changes in the inclusion level of exon 8 of MACF1 also occur in breast cancer. Changes in APP exon 8 and NUMB exon 9 AS appear to be more widespread. This conclusion is further supported by the detection of AS changes involving the latter two exons in automated RT-PCR screens of splicing changes in tumor samples from ovarian and breast cancer patients (27, 50). Importantly, despite the relatively high levels of inclusion of NUMB exon 9 in normal breast and colon tissues, our results show that this exon displays further increases in inclusion level in tumors from these tissues. Similarly, exon 8 in APP transcripts shows decreased inclusion levels in breast and colon tumors relative to those in the corresponding normal tissues from the same patients (Fig. 3B).

The detection of the APP and NUMB tumor-associated AS events in NSCLC, breast, and ovarian tumors (27, 50; this study) suggests that additional AS changes previously detected in other cancers may also occur in NSCLC. To assess this, we used RT-PCR assays to analyze 12 tumor-associated AS events (in transcripts from the *BTC*, *DNMT3B*, *FANCA*, *MCL1*, *STIM1*, *FGFR2*, *CADM1*, *PAXIP1*, *PLD1*, *SYNE2*, *TUBA4A*, and *UTRN* genes) previously detected in breast and ovarian tumors (27, 50) to determine whether they also occur in NSCLC adenocarcinomas profiled in the present study. Of these 12 AS events, five (PLD1, DNMT3B, SYNE2, UTRN, and FGFR2) were found to display changes in the inclusion level in three or more of five patient-matched pairs of normal lung and NSCLC adenocarcinoma tumor tissue (see Fig. S5 in the supplemental material). These results further support the existence of AS changes that occur in multiple tumor types and also emphasize the importance of implementing technologies that have broad detection coverage and sensitivity in order to widely capture such events (refer to Discussion).

Detection of NUMB exon 9-included splice variants at the protein level. Our data show that increased inclusion of NUMB exon 9 is the most widespread AS event among the 37 pairs of matched normal and tumor samples, derived from lung, breast, and colon tissues. In order to investigate the functional role of this tumor-associated AS event and also to further assess its potential utility as a cancer biomarker, we next determined whether it is differentially expressed between patient-matched normal and tumor tissues at the protein level.

Exon 9 AS affects coding sequences overlapping the functionally uncharacterized proline-rich-region (PRR) of the NUMB protein (Fig. 1B), with inclusion and skipping of the exon resulting in expression of NUMB isoforms referred to as "PRR-long" (PRR^L) and "PRR-short" (PRR^S), respectively (18). Where available in sufficient quantities for analysis (patient samples P1, P2, P8, and P10 in Fig. 2A), protein lysates from normal and matched tumor tissue were immunoblotted using two different rabbit polyclonal antibodies (18), one that recognizes both NUMB PRR^S and PRR^L isoforms but not NUMB-like protein ("pan isoform," raised against amino acids 499 to 518 of NUMB) and another that specifically recognizes PRR^L ("exon 9 coding," raised against amino acids 386 to 402, located in the PRR domain). A representative immunoblot performed on samples from patient P2, probed sequentially with the two antibodies, is shown in Fig. 4A.

The pan NUMB isoform antibody predominantly detected an isoform migrating at ~66 kDa in normal tissue lysates, consistent with previous reports (18), and RT-PCR assays in the present study indicating that an exon 9-skipped variant(s) encodes this form and is predominantly expressed in normal tissues (Fig. 2 and 3). In contrast, in tumor tissues, increased levels of a form of NUMB migrating at ~72 kDa and reduced levels of the ~66-kDa-migrating form were detected (Fig. 4A, top panel). Confirming that the ~72-kDa-migrating species represents PRR^L isoforms of NUMB, the blot in Fig. 4A was stripped and reprobed with the PRR^L-specific antibody (Fig. 4A, middle panel). As expected, this revealed a single band migrating at ~72 kDa. The average percentages of total mRNA and protein that correspond to exon 9-skipped PRR^S and exon 9-included PRR^L variants in the four pairs of patient-matched normal and tumor tissue are shown in Fig. 4B. The results in Fig. 4A and B confirm that PRR^L splice variants of NUMB are generally expressed at higher levels in NSCLC adenocarcinoma tumor tissue than in adjacent normal lung tissue.

Reduced expression of NUMB as a consequence of increased exon 9 inclusion. A comparison of the relative levels of NUMB splice variants at the RNA and protein levels between matched normal and tumor samples revealed a variable but consistent trend in which the ratios of PRR^L to PRR^S isoforms at the protein level are less than the ratios of exon 9-included to exon 9-skipped variants at the RNA level (Fig. 4C). After normalizing protein levels between normal and tumor tissues (using α-tubulin detection) and quantifying the total levels of the NUMB protein contributed by expression of both PRR^S and PRR^L isoforms, it is also apparent that there is a decrease in overall NUMB protein expression in tumor tissues relative to normal tissues. The total levels of NUMB isoforms at the RNA level do not show such a decrease. On average, the level of total NUMB protein is 2- to 3-fold lower in tumor tissue than in normal tissue (Fig. 4D). This observation is consistent with previous reports of reduced NUMB expression in NSCLCs (57) and breast tumors (38). Our combined results revealing tumor-associated increases in exon 9 inclusion and that PRR^L isoforms of NUMB are less well expressed at steady-state levels than PRR^S isoforms could therefore account, at least in part, for previous observations of reduced total NUMB expression in tumors.

To further investigate whether NUMB PRR^L isoforms are less well expressed at steady-state levels than PRR^S isoforms relative to the levels of expression of mRNAs encoding these isoforms, we transfected into lung A549 cells equal amounts of the NUMB cDNA expression plasmids "myc-NUMB-exon9-plus" and "myc-NUMB-exon9-minus" (containing and lacking exon 9, respectively) (lanes 2 to 4 and 5 to 7 in Fig. 5A and B). RNA and protein were harvested and analyzed by RT-PCR and by immunoblotting with the pan NUMB isoform antibody. Bar plots were generated to quantify mRNA (Fig. 5A) and protein isoform expression levels (Fig. 5B) relative to levels of the endogenous isoforms detected in the lanes corresponding

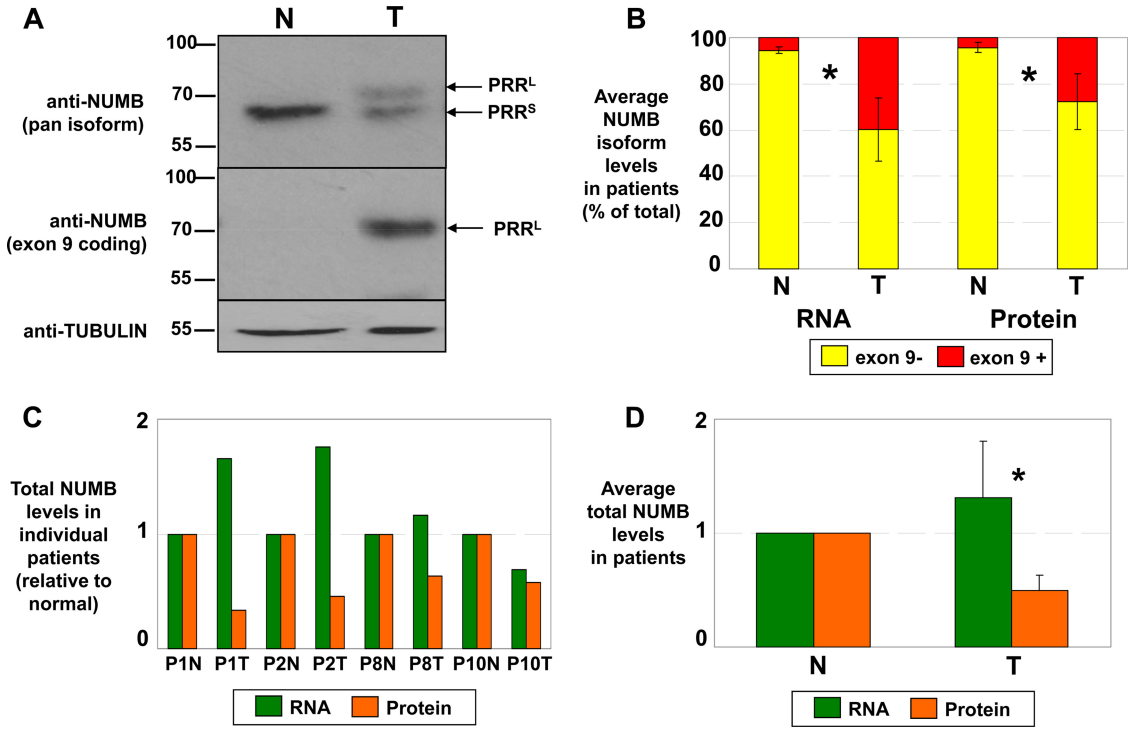

FIG. 4. Detection of tumor-associated changes in NUMB AS and expression at the protein level. (A) Patient lysates from normal (N) and tumor (T) tissue were first immunoblotted with an antibody detecting all NUMB isoforms ("pan isoform" antibody). The blot was stripped and reprobed with an antibody specific for exon 9 coding sequences located within the PRR domain ("exon 9 coding" antibody). Tubulin levels are shown as a control for sample loading and recovery. (B) Percentages of total NUMB mRNA and protein corresponding to exon 9-included/PRR^L and exon 9-skipped/PRR^S splice isoforms are shown as average measurements from four matched pairs of normal and tumor samples, with standard deviations indicated. (C) Bar plot comparing levels of total NUMB mRNA and protein in tumor tissue relative to the levels of total NUMB mRNA and protein in normal tissue (normalized to 1.0) for four different patients. (D) Average amounts of total NUMB mRNA and protein in tumor tissues from the four patient samples analyzed in panel B relative to the levels in the corresponding normal tissues (normalized in each case to 1.0). Measurements shown in panels B and C are from three independent analyses, and average values differing significantly ($P < 0.05$; Student's t test) are indicated with asterisks.

to transfected empty expression vector (lanes 1 in Fig. 5A and B) and relative to endogenous β-actin and α-tubulin levels, respectively. Consistent with results from the analysis of normal and tumor tissue samples in Fig. 4, the levels of the exon 9-included and exon 9-skipped mRNA isoforms were not significantly different from each other over three different amounts of each transfected plasmid. In contrast, the ratios of the PRR^L to PRR^S protein isoforms were significantly reduced (by 3.8- to 4.7-fold) over the three plasmid concentrations. These results support the conclusion that PRR^L isoforms of NUMB are less well expressed steady state than are PRR^S isoforms and that these differences therefore contribute to overall reduced levels of NUMB protein in tumor tissue relative to those in normal tissue.

Effect of reduced NUMB expression on Notch signaling. Previous observations support a role for NUMB in the suppression of the Notch signaling pathway (22, 38, 57), and a recent study has provided evidence suggesting that reduced NUMB levels may be associated with activation of Notch target genes in lung adenocarcinoma (57). We therefore reasoned that tumor-associated increases in NUMB exon 9 inclusion observed in the present study might contribute to Notch pathway activation. To investigate this possibility, we asked whether individual Notch target genes are upregulated in response to changes in the relative ratios of the PRR^L and PRR^S isoforms of NUMB.

The Notch target gene *HEY2* displays increased mRNA expression in 8 of 10 tumor tissues relative to that in the matched normal tissues from the patients analyzed earlier. However, we did not observe a direct correlation between the degree of the tumor-associated increases in %In levels for NUMB exon 9 and the increased levels of *HEY2* mRNA expression (Fig. 6A). Moreover, two other reported Notch target genes, *HES1* and *HEY1*, did not display increased expression in more than a few of the analyzed patients (Fig. 6A). These results therefore suggest that increased expression of PRR^L relative to that of PRR^S and/or decreased overall NUMB expression may contribute to the activation of specific Notch targets but not others. However, factors other than the relative levels of NUMB isoforms in tumor tissues likely function to establish the overall steady-state levels of specific Notch targets.

To more directly assess whether differential expression of NUMB PRR^L and PRR^S isoforms affect Notch target gene expression, we next assayed changes in mRNA expression of *HES1*, *HEY1*, and *HEY2* upon increased expression of each NUMB isoform in A549 cells, using the same sets of RNA samples as shown in Fig. 5 (Fig. 6B). Increased expression of

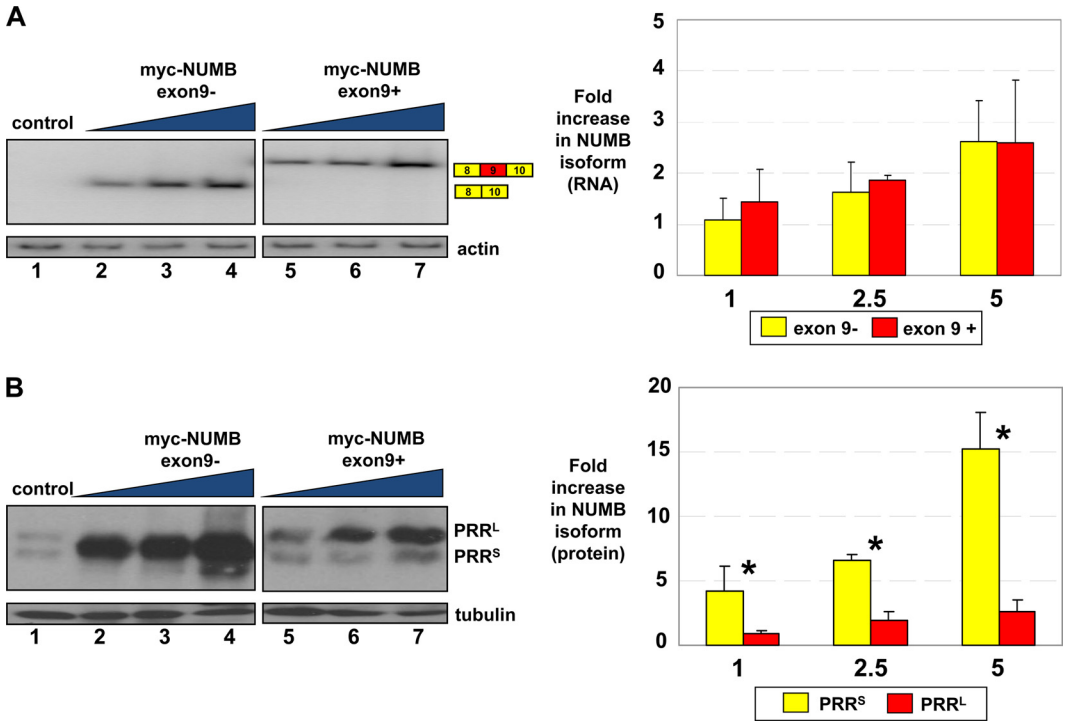

FIG. 5. Differences between mRNA and protein expression levels of NUMB splice isoforms. Three different amounts of expression plasmids for Myc-epitope-tagged NUMB, with or without inclusion of exon 9 (myc-NUMB-exon9-plus and myc-NUMB-exon9-minus, respectively), were transfected into lung A549 cells. RNA and protein isolated from the cells were analyzed for expression of each isoform. (A) RT-PCR assays showing levels of NUMB exon 9-included and -skipped isoforms. (B) Immunoblots analyzing NUMB isoform levels from the same samples as shown in panel A, probed with the pan-NUMB isoform antibody. Quantification of fold differences in mRNA and protein isoform levels over background (endogenous levels) and relative to levels of β-actin and α-tubulin controls, respectively, are shown in the adjacent bar plots. Fold differences are represented as averaged values from four independent transfection experiments, and standard deviations are shown. Amounts of plasmids transfected in panels A and B are as follows: 5 μg empty vector (lanes 1), 1 μg NUMB expression plasmid (lanes 2 and 5), 2.5 μg NUMB expression plasmid (lanes 3 and 6), and 5 μg NUMB expression plasmid (lanes 4 and 7). Values differing significantly ($P < 0.05$; Student's t test) are indicated with an asterisk.

the PRR^S isoform did not significantly alter mRNA levels of these Notch target genes. In contrast, increased expression of the PRR^L isoform consistently resulted in activation of *HEY1* and *HEY2* but not *HES1* mRNA expression (Fig. 6B). These results suggest that increased levels of the PRR^S isoform maintain suppression of Notch targets whereas increased expression of the PRR^L isoform is capable of negating this suppressive activity.

Next, we stably expressed an shRNA in A549 cells targeting the 3′-UTR of NUMB transcripts such that all isoforms were knocked down (Fig. 7A, compare lanes 1 and 2) and then introduced cDNA expression vectors to individually restore expression of each of these isoforms (lanes 3 and 4). Knockdown of all NUMB isoforms resulted in increased expression of all three Notch target genes assayed above (Fig. 7B). Selective "rescue" expression of the PRR^S isoform suppressed expression of the three Notch targets. However, selective expression of the PRR^L isoform did not suppress expression of the three Notch targets. Taken together, the results in Fig. 6 and 7 support the conclusion that the PRR^L isoform of NUMB lacks the capacity to suppress Notch activity and may act in a dominant manner to prevent the Notch suppressive activity of the PRR^S isoform. The latter conclusion is supported by the combined results of Fig. 5B and 6B, where the lowest level of PRR^L overexpression was sufficient to prevent the suppression of *HEY1* and *HEY2* by endogenous levels of the PRR^S isoform (compare lanes 1 and 5 in Fig. 5B with the corresponding columns in the bar graph in Fig. 6B).

Effect of NUMB isoforms on cell proliferation. Previous studies have suggested links between differential expression of NUMB PRR^S and PRR^L isoforms and transitions between cell proliferation and differentiation (see Discussion). It is therefore interesting to consider that increased inclusion of NUMB exon 9 may contribute to the proliferative capacity of tumor cells. To investigate this possibility, we first asked whether there is a direct correlation between the cell proliferation rate and the %In level of NUMB exon 9. To assess this, we compared previously established (43) "proliferation index" (PI) values of 16 different cell lines and tissues for which we have measured NUMB exon 9 %In levels in the present study. The PI values were previously derived as z scores representing expression levels (determined from published microarray data) of genes involved in cell proliferation in different cell/tissue types over the average expression levels of the same genes across a diverse panel of reference cell and tissue types (43). These values were shown to correlate well with known doubling rates of different cell types (43). By directly comparing the PI values to %In values for the 16 cell and tissue types

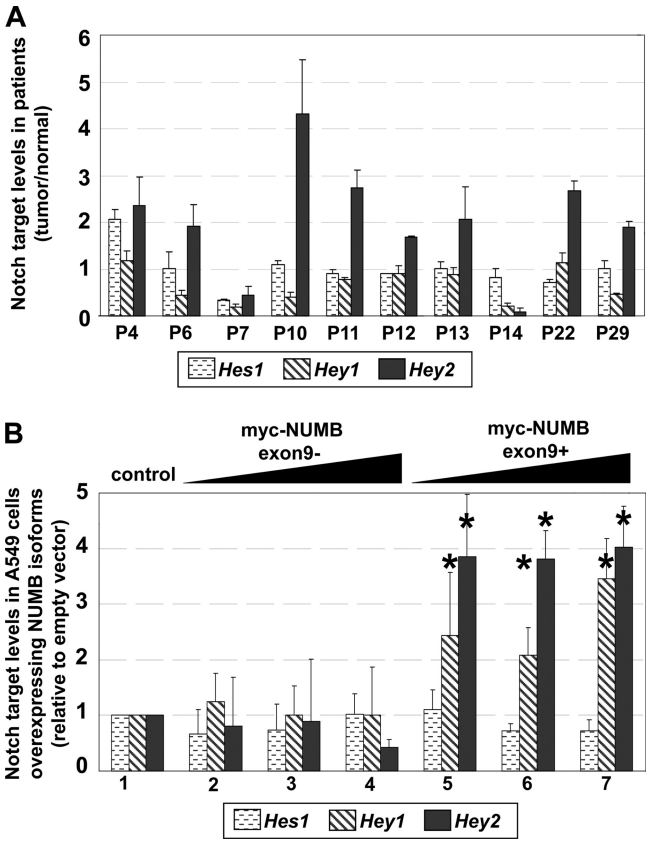

FIG. 6. Differential activities of NUMB splice isoforms in Notch signaling. (A) RT-PCR assays comparing mRNA levels of three Notch target genes (*HES1*, *HEY1*, and *HEY2*) in matched pairs of normal lung and NSCLC adenocarcinoma tissue from 10 of the patients analyzed in Fig. 2 and 3. All values are represented as a ratio of tumor/normal. (B) Effect of overexpression of exon 9-skipped/PRR^S and exon 9-included/PRR^L NUMB splice variants on Notch target genes in A549 cells, using the same samples analyzed in Fig. 5.

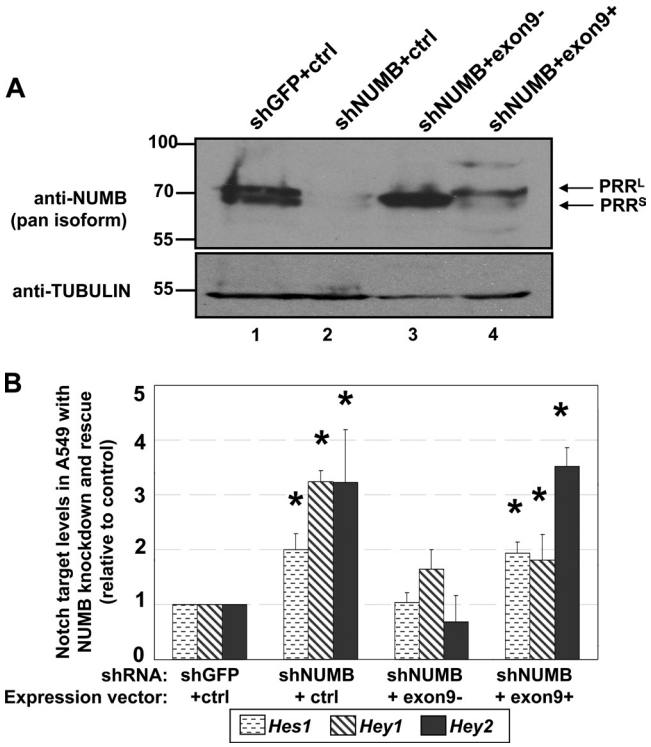

FIG. 7. Notch target gene mRNA levels in A549 cells following knockdown of all NUMB isoforms and isoform-specific rescue. Short hairpin RNAs targeting GFP (shGFP) (lane 1) and all NUMB isoforms (shNUMB) (lanes 2 to 4) were stably expressed together with a control (empty) expression vector (lanes 1 and 2), an expression vector for NUMB lacking exon 9 (myc-NUMB-exon9-minus) (lane 3), or an expression vector for NUMB containing exon 9 (myc-NUMB-exon9-plus) (lane 4). (A) Western blots showing detection of NUMB isoforms probed with the pan-NUMB isoform antibody and α-tubulin in the same samples (as a recovery/loading control). (B) Bar plot quantifying mRNA levels of the Notch target genes *HES1*, *HEY1*, and *HEY2* in each sample, as assayed by RT-PCR assays. mRNA levels of the Notch targets were normalized using β-actin mRNA levels and plotted as a fold change relative to levels in the shGFP expressing control. Values in the bar plots represent averages from three independent RT-PCR assays, and standard deviations are shown. Fold differences that are significantly different ($P < 0.05$; Student's t test) from the shGFP-expressing control are indicated with asterisks.

analyzed in the present study, we observe a statistically significant Pearson correlation coefficient (PCC) between the two measurements of 0.68 ($P < 0.004$). Given that both the PI and %In values are both semiquantitative and are derived from different cell/tissue samples, it is likely that this PCC value underrepresents the true level of correlation between NUMB exon 9 inclusion levels and the proliferation rate of cells. Nevertheless, we conclude that there is a significant positive correlation between NUMB exon 9 inclusion levels and cell proliferation rates.

To investigate whether cell doubling rates are influenced by increased levels of NUMB exon 9 inclusion, we next used a colorimetric assay to measure proliferation rates for the cell lines shown in Fig. 7 stably expressing a NUMB-targeting shRNA, with or without cDNAs for expression of each NUMB splice isoform (Fig. 8B). Each cell line was plated at the same density after a limited initial passage number (to avoid selection of possible compensatory mechanisms that might reduce NUMB-dependent effects), and proliferation rates were measured after 3 and then 6 days postplating.

After 6 days in culture, a significant increase in cell doublings was detected for the line expressing NUMB shRNA together with empty control vector (shNUMB+ctrl) compared to that of the parental A549 cell line or a control A549 cell line expressing shRNA targeted to GFP together with empty vector (shGFP+ctrl). Knockdown of NUMB in combination with expression of the PRR^L isoform (shNUMB+exon9+) resulted in an increase in the cell doubling rate comparable to that of the shNUMB+ctrl-expressing cell line. In contrast, knockdown of NUMB together with expression of the PRR^S isoform (shNUMB+exon9−) significantly reduced cell doubling rates compared to those when the PRR^L isoform was expressed or to those when both NUMB isoforms were knocked down. These results support the conclusion that increased inclusion of NUMB exon 9 and consequent increased expression of the NUMB PRR^L isoform relative to that of the PRR^S isoform increases cell proliferation rates. It is therefore possible that mechanisms which promote increased inclusion of NUMB

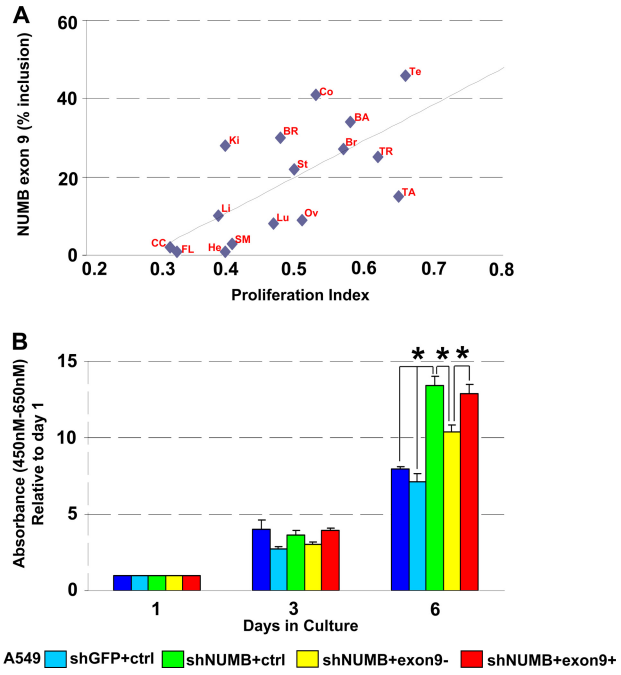

FIG. 8. Relationship between NUMB isoform expression and cell proliferation rates. (A) Correlation analysis of RT-PCR-quantified NUMB exon 9 %In levels versus proliferation index values of 16 different cell lines and tissues (as determined in reference 43). The Pearson correlation coefficient for the 16 pairs is 0.68 ($P < 0.004$). Te, testis; Co, colon; BA, B-cell (activated); BR, B-cell (resting); Ki, kidney; Br, breast; TR, t-cell (resting); St, stomach; TA, T-cell (activated); Li, liver; Ov, ovary; Lu, lung; SM, skeletal muscle; CC, cerebral cortex; FL, frontal lobe; He, heart. (B) Cell proliferation was monitored using a colorimetric assay (refer to Materials and Methods) for untransfected A549 cells and for the A549 cell lines stably expressing a NUMB-targeting shRNA with or without stable expression of NUMB isoform cDNAs, as shown in Fig. 7. Quantification of above-background absorbance at 450 nM was used to monitor changes in cell density for each cell line relative to levels on day 1 (normalized to 1.0). Average absorbance values and standard deviations were measured from 12 technical replicates from three independent transfection experiments. Values differing significantly ($P < 0.05$; Student's t test) are indicated with an asterisk.

exon 9 may contribute to the proliferative capacity of tumor cells.

DISCUSSION

Using quantitative AS microarray profiling, we detected alternative exons in transcripts from the *VEGFA*, *MACF1*, *APP*, and *NUMB* genes that display frequent changes in inclusion level in adenocarcinoma tumors from patients with NSCLC. Additionally, the same alternative exons in the *APP* and *NUMB* genes were found to undergo changes in inclusion level in tumors from breast and colon cancer patients. The most widespread AS change was a tumor-associated increase in inclusion of exon 9 of *NUMB* transcripts. Increased expression of exon 9-included NUMB splice isoforms in tumors was detected at the protein level and linked to a reduction in overall levels of the NUMB protein, activation of the Notch signaling pathway, and increased cell proliferation. Coupled with previous results demonstrating a role for Notch activation in cancers, our results reveal a possible mechanism by which a change in AS may contribute to tumorigenesis and further reveal tumor-associated AS events that represent targets with potential clinical utility.

New links between AS and tumorigenesis. Of the four lung adenocarcinoma-associated AS events identified in our study, only VEGFA transcripts with altered inclusion levels of exons 6 and/or 7 have been previously identified in NSCLC (26, 59, 62). VEGFs are important signaling proteins that promote *de novo* vascularization during development of the embryonic circulatory system and also stimulate blood vessel growth (angiogenesis) in tumor tissues. The known VEGF isoforms are depicted in Fig. S3 in the supplemental material. Based on the results of heparin binding assays, splice isoforms including exons 6 and 7 are thought to be tightly bound to the extracellular matrix (ECM), whereas isoforms including one of these two exons have moderate ECM interaction, and isoforms that skip these exons are freely secreted (20). The differential expression of these isoforms in NSCLC has been assessed as a possible prognostic indicator, with promising results (48, 59). Our results further support the conclusion that differential AS of VEGFA transcripts may be an important step in the growth and spread of tumors in patients with NSCLC. However, based on our initial profiling of colon and breast tumors, this mechanism may not occur or is less prevalent in these cancer types.

MACF1 belongs to the plakin family of cytoskeletal linker proteins. It is a large cytoskeletal protein that forms bridges between different cytoskeletal elements through its modular domains, which bind actin and microtubules. Alternatively spliced transcripts of MACF1 have been previously described (2, 32) but do not involve the AS event we have detected in the present study. While MACF1 has not been directly implicated in cancer, it has been reported to function in the Wnt signaling pathway, of which various components have been linked to tumorigenesis (41, 54). MACF1 is associated with a complex containing Axin, beta-catenin, glycogen synthase kinase 3β (GSK3β), and adenomatous polyposis coli (APC). Depletion of MACF1 results in decreased levels of beta-catenin in the nucleus and reduced levels of TCF/beta-catenin transcriptional activation (11). It is interesting to consider that increased inclusion of the alternative exon we have detected in MACF1 transcripts in lung adenocarcinoma and breast tumor tissues may contribute to altered Wnt signaling in cancers.

APP is an integral and widely expressed membrane protein that normally functions in the regulation of synapse formation and neural plasticity (12, 16). APP is initially expressed as a precursor protein which undergoes proteolysis via secretases to generate a soluble NH_2-terminal ectodomain fragment (sAPP), an amyloid beta (A4) peptide (APP), and cytosolic COOH-terminal fragments. The A4 peptide is a primary component of amyloid plaques in the brains of Alzheimer's disease (AD) patients (37). Reported splice isoforms of APP arise through variable inclusion of exons 7, 8, and 15, with increased inclusion of exon 7 detected in AD patients (24, 45). In addition to its role in AD, increased expression of APP and sAPP has been linked to

cell proliferation and tumorigenesis in prostate, pancreatic, thyroid, and oral squamous cell cancers (23, 28, 29, 47). Our results reveal that exon 8 but not exon 7 undergoes increased skipping in tumors from lung, breast, and colon cancer patients. While the specific role of APP exon 8 at the protein level is not known, it is interesting to consider that the loss of inclusion of this exon in cancers could affect the relative levels of the different cleavage products of APP, which in turn might contribute to the possible tumorigenic properties of this gene (40).

The widespread tumor-associated AS change in NUMB transcripts was specific to exon 9, since inclusion levels of exon 3, the only other known alternatively spliced exon in NUMB transcripts, did not differ significantly between patient normal and tumor samples (see Fig. S4 in the supplemental material). The coding sequence of exon 9 overlaps the proline-rich region (PRR) of NUMB (Fig. 1B), the function of which is unknown. However, it has been reported that increased levels of PRR^L NUMB isoforms can promote proliferation of embryo-derived cell lines whereas the expression of these isoforms declines following differentiation (1, 18, 19, 52, 58). These findings, coupled with our results supporting a specific role for NUMB exon 9-included/PRR^L isoforms in increased cell proliferation, suggest that increased levels of exon 9 inclusion in NUMB may function to promote cell proliferation both during development and during tumorigenesis. The "reactivation" of AS patterns in cancer that normally function during development is a reoccurring theme in cancer, with notable other examples involving VEGFA alternative exons 6 and 7 and the middle variable exons of the CD44 gene (30, 33).

Altered regulation of *NUMB* and *NOTCH* has been implicated in cancers (25, 38). Recently, an RNA interference (RNAi)-based screen identified NUMB as having tumor suppressor activity in a mouse lymphoma model (6). Moreover, highly reduced or absent NUMB protein expression was detected in at least one-third of analyzed NSCLC tumors (including both adenocarcinomas and squamous cell carcinomas), and an inverse correlation was observed between the levels of NUMB and activated Notch1 (57). Taken together with the detection of increased inclusion levels of exon 9 in NSCLC adenocarcinomas (this study) and in other cancer types (27, 50; this study), as well as the finding that the exon 9-included, PRR^L splice variants of NUMB are specifically expressed at elevated levels in tumor tissue at the expense of overall NUMB protein expression, a possible mechanistic model for the role of NUMB exon 9 in cancer emerges.

In this model, changes in the activity of one or more AS regulators during tumorigenesis lead to increased inclusion of exon 9. This increased level of exon 9 splicing causes overall NUMB levels to be reduced with subsequent Notch activation. In light of the results of the cDNA expression experiments in the present study, it is also possible that the PRR^L splice isoform acts in a dominant manner to suppress the Notch inhibitory activity of the PRR^S splice isoform. A consequence of decreased overall NUMB expression and/or increased expression of the PRR^L splice isoform is increased cell proliferation. Thus, out-of-context AS of NUMB exon 9 may account, at least in part, for the increased proliferative capacity of tumor cells. A future challenge will be to define the mechanism(s) responsible for the tumor-associated changes in AS of NUMB exon 9 and also for other AS events linked to cancer that have been identified. In this regard, it is interesting to note that a recent study has provided evidence that the splicing regulators Nova and Fox2 function in the regulation of NUMB exon 9 AS (60), and downregulation of Fox2 expression has been linked to AS changes in ovarian cancer (51), although we did not detect a significant change in its expression level between the matched NSCLC tumor and normal lung tissues surveyed in the present study.

Our study, together with those of other groups, emphasizes the importance of quantitatively profiling AS in cancer. Changes in this gene regulatory layer clearly play important mechanistic roles in tumorigenesis, yet most tumor-associated AS events have not been functionally characterized on any level and many others likely remain to be discovered. For example, while our profiling system afforded sensitive detection of relatively pronounced tumor-associated AS events that occur in the majority of patients, it did not provide comprehensive coverage of annotated AS events. Similarly, while automated RT-PCR-based screens are capable of more-sensitive detection of relatively smaller tumor-associated changes in exon inclusion levels, to date these screens have been focused on selected subsets of human genes and annotated AS events and therefore likely also missed important cancer-associated AS events (27, 50). Future cancer and other disease profiling studies will benefit from the use of high-throughput RNA sequencing, since this technology can yield data sets with greater coverage of the transcriptome as well as greater quantitative accuracy (4, 55).

ACKNOWLEDGMENTS

We thank Ofer Shai, Qun Pan, Leo Lee, and Joseph Calarco for assistance with experiments and analysis and Arneet Saltzman, Bushra Raj, John Calarco, Mathieu Gabut, and Nebojsa Jojic for helpful suggestions and comments on the manuscript.

This research was funded by grants from the Canadian Cancer Society to B.J.B. (NCIC no. 012169) and M.S.T. (NCIC no. 012150) and grants from the Canadian Institutes of Health Research (MOP-67011), the Ontario Research Fund, and Microsoft Research and Genome Canada through the OGI to B.J.B. and others.

We have no potential conflicts of interest to disclose.

REFERENCES

1. **Bani-Yaghoub, M., C. J. Kubu, R. Cowling, J. Rochira, G. N. Nikopoulos, S. Bellum, and J. M. Verdi.** 2007. A switch in numb isoforms is a critical step in cortical development. Dev. Dyn. **236:**696–705.
2. **Bernier, G., M. Pool, M. Kilcup, J. Alfoldi, Y. De Repentigny, and R. Kothary.** 2000. Acf7 (MACF) is an actin and microtubule linker protein whose expression predominates in neural, muscle, and lung development. Dev. Dyn. **219:**216–225.
3. **Blencowe, B. J.** 2006. Alternative splicing: new insights from global analyses. Cell **126:**37–47.
4. **Blencowe, B. J., S. Ahmad, and L. J. Lee.** 2009. Current-generation high-throughput sequencing: deepening insights into mammalian transcriptomes. Genes Dev. **23:**1379–1386.
5. **Blencowe, B. J., R. Issner, J. A. Nickerson, and P. A. Sharp.** 1998. A coactivator of pre-mRNA splicing. Genes Dev. **12:**996–1009.
6. **Bric, A., C. Miething, C. U. Bialucha, C. Scuoppo, L. Zender, A. Krasnitz, Z. Xuan, J. Zuber, M. Wigler, J. Hicks, R. W. McCombie, M. T. Hemann, G. J. Hannon, S. Powers, and S. W. Lowe.** 2009. Functional identification of tumor-suppressor genes through an in vivo RNA interference screen in a mouse lymphoma model. Cancer Cell **16:**324–335.
7. **Caceres, J. F., and A. R. Kornblihtt.** 2002. Alternative splicing: multiple

control mechanisms and involvement in human disease. Trends Genet. **18:** 186–193.
8. **Calarco, J. A., S. Superina, D. O'Hanlon, M. Gabut, B. Raj, Q. Pan, U. Skalska, L. Clarke, D. Gelinas, D. van der Kooy, M. Zhen, B. Ciruna, and B. J. Blencowe.** 2009. Regulation of vertebrate nervous system alternative splicing and development by an SR-related protein. Cell **138:**898–910.
9. **Calarco, J. A., Y. Xing, M. Cáceres, J. P. Calarco, X. Xiao, Q. Pan, C. Lee, T. M. Preuss, and B. J. Blencowe.** 2007. Global analysis of alternative splicing differences between humans and chimpanzees. Genes Dev. **21:**2963–2975.
10. **Castle, J., P. Garrett-Engele, C. D. Armour, S. J. Duenwald, P. M. Loerch, M. R. Meyer, E. E. Schadt, R. Stoughton, M. L. Parrish, D. D. Shoemaker, and J. M. Johnson.** 2003. Optimization of oligonucleotide arrays and RNA amplification protocols for analysis of transcript structure and alternative splicing. Genome Biol. **4:**R66.
11. **Chen, H.-J., C.-M. Lin, C.-S. Lin, R. Perez-Olle, C. L. Leung, and R. K. H. Liem.** 2006. The role of microtubule actin cross-linking factor 1 (MACF1) in the Wnt signaling pathway. Genes Dev. **20:**1933–1945.
12. **Chen, Y., and B. L. Tang.** 2006. The amyloid precursor protein and postnatal neurogenesis/neurogeneration. Biochem. Biophys. Res. Commun. **341:**1–5.
13. **Chomczynski, P., and N. Sacchi.** 1987. Single-step method of RNA isolation by acid guanidinium thiocyanate-phenol-chloroform extraction. Anal. Biochem. **162:**156–159.
14. **Clower, C. V., D. Chatterjee, Z. Wang, L. C. Cantley, M. G. Vander Heiden, and A. R. Krainer.** 2010. The alternative splicing repressors hnRNP A1/A2 and PTB influence pyruvate kinase isoform expression and cell metabolism. Proc. Natl. Acad. Sci. U. S. A. **107:**1894–1899.
15. **Cooper, T. A., L. Wan, and G. Dreyfuss.** 2009. RNA and disease. Cell **136:**777–793.
16. **Crews, L., E. Rockenstein, and E. Masliah.** 2010. APP transgenic modeling of Alzheimer's disease: mechanisms of neurodegeneration and aberrant neurogenesis. Brain Struct. Funct. **214:**111–126.
17. **David, C. J., M. Chen, M. Assanah, P. Canoll, and J. L. Manley.** 2010. HnRNP proteins controlled by c-Myc deregulate pyruvate kinase mRNA splicing in cancer. Nature **463:**364–368.
18. **Dho, S. E., M. B. French, S. A. Woods, and C. J. McGlade.** 1999. Characterization of four mammalian numb protein isoforms. Identification of cytoplasmic and membrane-associated variants of the phosphotyrosine binding domain. J. Biol. Chem. **274:**33097–33104.
19. **Dooley, C. M., J. James, C. J. McGlade, and I. Ahmad.** 2003. Involvement of numb in vertebrate retinal development: evidence for multiple roles of numb in neural differentiation and maturation. J. Neurobiol. **54:**313–325.
20. **Gitay-Goren, H., S. Soker, I. Vlodavsky, and G. Neufeld.** 1992. The binding of vascular endothelial growth factor to its receptors is dependent on cell surface-associated heparin-like molecules. J. Biol. Chem. **267:**6093–6098.
21. **Glatz, D. C., D. Rujescu, Y. Tang, F. J. Berendt, A. M. Hartmann, F. Faltraco, C. Rosenberg, C. Hulette, K. Jellinger, H. Hampel, P. Riederer, H. J. Moller, A. Andreadis, K. Henkel, and S. Stamm.** 2006. The alternative splicing of tau exon 10 and its regulatory proteins CLK2 and TRA2-BETA1 changes in sporadic Alzheimer's disease. J. Neurochem. **96:**635–644.
22. **Gulino, A., L. Di Marcotullio, and I. Screpanti.** 2010. The multiple functions of Numb. Exp. Cell Res. **316:**900–906.
23. **Hansel, D. E., A. Rahman, S. Wehner, V. Herzog, C. J. Yeo, and A. Maitra.** 2003. Increased expression and processing of the Alzheimer amyloid precursor protein in pancreatic cancer may influence cellular proliferation. Cancer Res. **63:**7032–7037.
24. **Ho, L., K. Fukuchi, and S. G. Younkin.** 1996. The alternatively spliced Kunitz protease inhibitor domain alters amyloid beta protein precursor processing and amyloid beta protein production in cultured cells. J. Biol. Chem. **271:** 30929–30934.
25. **Katoh, M.** 2007. Networking of WNT, FGF, Notch, BMP, and Hedgehog signaling pathways during carcinogenesis. Stem Cell Rev. **3:**30–38.
26. **Keedy, V. L., and A. B. Sandler.** 2007. Inhibition of angiogenesis in the treatment of non-small cell lung cancer. Cancer Sci. **98:**1825–1830.
27. **Klinck, R., A. Bramard, L. Inkel, G. Dufresne-Martin, J. Gervais-Bird, R. Madden, E. R. Paquet, C. Koh, J. P. Venables, P. Prinos, M. Jilaveanu-Pelmus, R. Wellinger, C. Rancourt, B. Chabot, and S. Abou Elela.** 2008. Multiple alternative splicing markers for ovarian cancer. Cancer Res. **68:** 657–663.
28. **Ko, S. Y., S. C. Lin, K. W. Chang, Y. K. Wong, C. J. Liu, C. W. Chi, and T. Y. Liu.** 2004. Increased expression of amyloid precursor protein in oral squamous cell carcinoma. Int. J. Cancer **111:**727–732.
29. **Krause, K., S. Karger, S. Y. Sheu, T. Aigner, R. Kursawe, O. Gimm, K. W. Schmid, H. Dralle, and D. Fuhrer.** 2008. Evidence for a role of the amyloid precursor protein in thyroid carcinogenesis. J. Endocrinol. **198:**291–299.
30. **Krilleke, D., Y. S. Ng, and D. T. Shima.** 2009. The heparin-binding domain confers diverse functions of VEGF-A in development and disease: a structure-function study. Biochem. Soc. Trans. **37:**1201–1206.
31. **Le, K., K. Mitsouras, M. Roy, Q. Wang, Q. Xu, S. F. Nelson, and C. Lee.** 2004. Detecting tissue-specific regulation of alternative splicing as a qualitative change in microarray data. Nucleic Acids Res. **32:**e180.
32. **Lin, C., H. J. Chen, C. L. Leung, D. A. Parry, and R. K. Liem.** 2005. Microtubule actin crosslinking factor 1b: a novel plakin that localizes to the Golgi complex. J. Cell Sci. **118:**3727–3738.
33. **Naor, D., S. Nedvetzki, I. Golan, L. Melnik, and Y. Faitelson.** 2002. CD44 in cancer. Crit. Rev. Clin. Lab. Sci. **39:**527–579.
34. **Pan, Q., A. L. Saltzman, Y. K. Kim, C. Misquitta, O. Shai, L. E. Maquat, B. J. Frey, and B. J. Blencowe.** 2006. Quantitative microarray profiling provides evidence against widespread coupling of alternative splicing with nonsense-mediated mRNA decay to control gene expression. Genes Dev. **20:**153–158.
35. **Pan, Q., O. Shai, L. J. Lee, B. J. Frey, and B. J. Blencowe.** 2008. Deep surveying of alternative splicing complexity in the human transcriptome by high-throughput sequencing. Nat. Genet. **40:**1413–1415.
36. **Pan, Q., O. Shai, C. Misquitta, W. Zhang, A. L. Saltzman, N. Mohammad, T. Babak, H. Siu, T. R. Hughes, Q. D. Morris, B. J. Frey, and B. J. Blencowe.** 2004. Revealing global regulatory features of mammalian alternative splicing using a quantitative microarray platform. Mol. Cell **16:**929–941.
37. **Paris, D., A. Quadros, N. Patel, A. DelleDonne, J. Humphrey, and M. Mullan.** 2005. Inhibition of angiogenesis and tumor growth by beta and gamma-secretase inhibitors. Eur. J. Pharmacol. **514:**1–15.
38. **Pece, S., M. Serresi, E. Santolini, M. Capra, E. Hulleman, V. Galimberti, S. Zurrida, P. Maisonneuve, G. Viale, and P. P. Di Fiore.** 2004. Loss of negative regulation by Numb over Notch is relevant to human breast carcinogenesis. J. Cell Biol. **167:**215–221.
39. **Pio, R., and L. M. Montuenga.** 2009. Alternative splicing in lung cancer. J. Thorac. Oncol. **4:**674–678.
40. **Roncarati, R., N. Sestan, M. H. Scheinfeld, B. E. Berechid, P. A. Lopez, O. Meucci, J. C. McGlade, P. Rakic, and L. D'Adamio.** 2002. The gamma-secretase-generated intracellular domain of beta-amyloid precursor protein binds Numb and inhibits Notch signaling. Proc. Natl. Acad. Sci. U. S. A. **99:**7102–7107.
41. **Saadeddin, A., R. Babaei-Jadidi, B. Spencer-Dene, and A. S. Nateri.** 2009. The links between transcription, beta-catenin/JNK signaling, and carcinogenesis. Mol. Cancer Res. **7:**1189–1196.
42. **Sanchez-Cespedes, M.** 2009. Lung cancer biology: a genetic and genomic perspective. Clin. Transl. Oncol. **11:**263–269.
43. **Sandberg, R., J. R. Neilson, A. Sarma, P. A. Sharp, and C. B. Burge.** 2008. Proliferating cells express mRNAs with shortened 3′ untranslated regions and fewer microRNA target sites. Science **320:**1643–1647.
44. **Shai, O., Q. D. Morris, B. J. Blencowe, and B. J. Frey.** 2006. Inferring global levels of alternative splicing isoforms using a generative model of microarray data. Bioinformatics **22:**606–613.
45. **Shibata, A., M. Hattori, H. Suda, and Y. Sakaki.** 1996. Identification of cis-acting elements involved in an alternative splicing of the amyloid precursor protein (APP) gene. Gene **175:**203–208.
46. **Stav, D., I. Bar, and J. Sandbank.** 2008. Gene expression subtraction of non-cancerous lung from smokers and non-smokers with adenocarcinoma, as a predictor for smokers developing lung cancer. J. Exp. Clin. Cancer Res. **27:**45–52.
47. **Takayama, K.-I., S. Tsutsumi, T. Suzuki, K. Horie-Inoue, K. Ikeda, K. Kaneshiro, T. Fujimura, J. Kumagai, T. Urano, Y. Sakaki, K. Shirahige, H. Sasano, S. Takahashi, T. Kitamura, Y. Ouchi, H. Aburatani, and S. Inoue.** 2009. Amyloid precursor protein is a primary androgen target gene that promotes prostate cancer growth. Cancer Res. **69:**137–142.
48. **Tsao, M. S., N. Liu, T. Nicklee, F. Shepherd, and J. Viallet.** 1997. Angiogenesis correlates with vascular endothelial growth factor expression but not with Ki-ras oncogene activation in non-small cell lung carcinoma. Clin. Cancer Res. **3:**1807–1814.
49. **Venables, J. P.** 2006. Unbalanced alternative splicing and its significance in cancer. Bioessays **28:**378–386.
50. **Venables, J. P., R. Klinck, A. Bramard, L. Inkel, G. Dufresne-Martin, C. Koh, J. Gervais-Bird, E. Lapointe, U. Froehlich, M. Durand, D. Gendron, J.-P. Brosseau, P. Thibault, J.-F. Lucier, K. Tremblay, P. Prinos, R. J. Wellinger, B. Chabot, C. Rancourt, and S. A. Elela.** 2008. Identification of alternative splicing markers for breast cancer. Cancer Res. **68:**9525–9531.
51. **Venables, J. P., R. Klinck, C. Koh, J. Gervais-Bird, A. Bramard, L. Inkel, M. Durand, S. Couture, U. Froehlich, E. Lapointe, J.-F. Lucier, P. Thibault, C. Rancourt, K. Tremblay, P. Prinos, B. Chabot, and S. A. Elela.** 2009. Cancer-associated regulation of alternative splicing. Nat. Struct. Mol. Biol. **16:**670–676.
52. **Verdi, J. M., A. Bashirullah, D. E. Goldhawk, C. J. Kubu, M. Jamali, S. O. Meakin, and H. D. Lipshitz.** 1999. Distinct human NUMB isoforms regulate differentiation vs. proliferation in the neuronal lineage. Proc. Natl. Acad. Sci. U. S. A. **96:**10472–10476.
53. **Wang, E. T., R. Sandberg, S. Luo, I. Khrebtukova, L. Zhang, C. Mayr, S. F. Kingsmore, G. P. Schroth, and C. B. Burge.** 2008. Alternative isoform regulation in human tissue transcriptomes. Nature **456:**470–476.
54. **Wang, Y.** 2009. Wnt/Planar cell polarity signalling: a new paradigm for cancer therapy. Mol. Cancer Ther. **8:**2103–2109.
55. **Wang, Z., M. Gerstein, and M. Snyder.** 2009. RNA-Seq: a revolutionary tool for transcriptomics. Nat. Rev. Genet. **10:**57–63.
56. **Ward, A. J., and T. A. Cooper.** 2010. The pathobiology of splicing. J. Pathol. **220:**152–163.

57. **Westhoff, B., I. N. Colaluca, G. D'Ario, M. Donzelli, D. Tosoni, S. Volorio, G. Pelosi, L. Spaggiari, G. Mazzarol, G. Viale, S. Pece, and P. P. Di Fiore.** 2009. Alterations of the Notch pathway in lung cancer. Proc. Natl. Acad. Sci. U. S. A. **106:**22293–22298.
58. **Yoshida, T., A. Tokunaga, K. Nakao, and H. Okano.** 2003. Distinct expression patterns of splicing isoforms of mNumb in the endocrine lineage of developing pancreas. Differentiation **71:**486–495.
59. **Yuan, A., C. J. Yu, S. H. Kuo, W. J. Chen, F. Y. Lin, K. T. Luh, P. C. Yang, and Y. C. Lee.** 2001. Vascular endothelial growth factor 189 mRNA isoform expression specifically correlates with tumor angiogenesis, patient survival, and postoperative relapse in non-small-cell lung cancer. J. Clin. Oncol. **19:**432–441.
60. **Zhang, C., M. A. Frias, A. Mele, M. Ruggiu, T. Eom, C. B. Marney, H. Wang, D. D. Licatalosi, J. J. Fak, and R. B. Darnell.** 2010. Intergrative modeling defines the Nova splicing-regulatory network and its combinatorial controls. Science **329:**439–443.
61. **Zhang, C., H. R. Li, J. B. Fan, J. Wang-Rodriguez, T. Downs, X. D. Fu, and M. Q. Zhang.** 2006. Profiling alternatively spliced mRNA isoforms for prostate cancer classification. BMC Bioinformatics **7:**202.
62. **Zygalaki, E., E. G. Tsaroucha, L. Kaklamanis, and E. S. Lianidou.** 2007. Quantitative real-time reverse transcription PCR study of the expression of vascular endothelial growth factor (VEGF) splice variants and VEGF receptors (VEGFR-1 and VEGFR-2) in non small cell lung cancer. Clin. Chem. **53:**1433–1439.